Neuroradiology (2001) 43: 169–177
© Springer-Verlag 2001

A.A. Tzika
D. Zurakowski
T. Young Poussaint
L. Goumnerova
L.G. Astrakas
P.D. Barnes
D.C. Anthony
A.L. Billett
N.J. Tarbell
R.M. Scott
P.McL. Black

Proton magnetic spectroscopic imaging of the child's brain: the response of tumors to treatment

Received: 26 July 1999
Accepted: 27 July 2000

A.A. Tzika (✉) · T. Young Poussaint · L.G. Astrakas · P.D. Barnes
Department of Radiology,
Children's Hospital and Harvard Medical School, Boston, MA, USA

D. Zurakowski
Department of Biostatistics,
Children's Hospital and Harvard Medical School, Boston, MA, USA

L. Goumnerova · R.M. Scott · P.McL. Black
Department of Neurosurgery,
Children's Hospital and Harvard Medical School, Boston, MA, USA

D.C. Anthony
Department of Pathology,
Children's Hospital and Harvard Medical School, Boston, MA, USA

A.L. Billett · N.J. Tarbell
Department of Radiation Oncology,
Children's Hospital and Harvard Medical School, Boston, MA, USA

Present address: A.A. Tzika,
Department of Radiology,
Children's Hospital,
300 Longwood Avenue, Boston,
MA 02115, USA,
e-mail: tzika@a1.tch.harvard.edu
Tel.: + 1-617-3556521
Fax: + 1-617-7300465

Abstract Our aim was to determine and/or predict response to treatment of brain tumors in children using proton magnetic resonance spectroscopic imaging (MRSI). We studied 24 patients aged 10 months to 24 years, using MRI and point-resolved spectroscopy (PRESS; TR 2000 TE 65 ms) with volume preselection and phase-encoding in two dimensions on a 1.5 T imager. Multiple logistic regression was used to establish independent predictors of active tumor growth. Biologically vital cell metabolites, such as *N*-acetyl aspartate and choline-containing compounds (Cho), were significantly different between tumor and control tissues ($P < 0.001$). The eight brain tumors which responded to radiation or chemotherapy, exhibited lower Cho ($P = 0.05$), higher total creatine (tCr) ($P = 0.02$) and lower lactate and lipid (L) ($P = 0.04$) than16 tumors which were not treated (except by surgery) or did not respond to treatment. The only significant independent predictor of active tumor growth was tCr ($P < 0.01$). We suggest that tCr is useful in assessing response of brain tumors to treatment.

Key words Brain, tumors · Children · Magnetic resonance spectroscopy

Introduction

The incidence of cancer has risen in children less than 15 years of age in the USA [1]. This is largely due to increases in lymphoblastic leukemia and tumors of the nervous system. Between 1973 and 1988 the incidence of childhood tumors of the nervous system increased by 30 % [2]. Every year more than 1500 children are diagnosed as having brain tumors [3]. Because a child is more likely to develop cancer during the first 5 years of

life, the etiology of these early cancers is likely to be different from that of those later in life and probably the result of different factors. Tumors are more aggressive in children than in adults, but long-term disease control is often possible [4]. Despite an overall decrease in childhood mortality due to cancer, mortality due to nervous system cancer has decreased less than that of other childhood malignancies [1]. This suggests the need for better control and highlights the importance of evaluating improved treatment protocols for children with brain tumors. We anticipated that our study might provide important preliminary information on the metabolic characterization of childhood brain tumors and their response to treatment. Our long-term goal is to determine the clinical utility of serial MRI and MRS as part of an integrated approach for evaluation of treatment. MRI complemented by MRS may yield unique prospective information for the management of children's brain tumors.

Our previous studies have suggested that proton MR spectra acquired within brain tumors can be distinguished from those in control tissues of the same patients [5, 6, 7]. So far, we are in agreement with others who have used single-voxel MRS to study brain tumors in children [8, 9, 10, 11, 12, 13] and adults [14, 15, 16, 17, 18, 19, 20]. Additional reports using in vitro [10, 21, 22, 23, 24, 25, 26] and in vivo [15, 27, 28, 29, 30, 31, 32, 33, 34, 35] proton MRS have shown similar findings. Single-voxel MRS is useful in tumor detection and possibly differentiation of tumor types, adding to greater specificity of MRI imaging in the preoperative assessment of tumors [6, 20, 36, 37, 38, 39].

In order to assess treated tumors, multivoxel spectroscopic techniques, permitting spectroscopic imaging, were needed in the clinical setting. Clinical implementation of such a technique, two-dimensional chemical shift imaging (CSI) [40], has been accomplished. This has shown that the clinical value of MRS may include not only differential diagnosis of brain neoplasms [39] but also monitoring of therapy [41, 42]. The clinical question is whether MRS can aid in detection of response to therapy and in differentiation of tumor recurrence from treatment effects [38].

We employed a two-dimensional CSI technique to identify biologically significant indices of response of tumors to therapy and predictors of active tumor growth within the tumor bed. We postulated that MRS could be used with MRI in detecting response to therapy.

Materials and methods

We examined 24 patients (11 females and 13 males) aged 10 months to 24 years with brain tumors of neuroepithelial origin (Table 1) on a 1.5 T system, using two-dimensional CSI proton MRS. Permission was obtained from the parents of all subjects. The MRS findings were analyzed in the context of MRI, histopathology, and clinical findings.

Of the 24 patients, patients 1–8 had tumors treated only by surgery, patients 9–16 had tumors treated by radiation or chemotherapy with recurrence, and patients 17–24 had tumors treated without recurrence.

We grouped recurrent and untreated tumors as growing or active tumors (AT) (Table 2). Tumors treated and showing no signs of recurrence were classed as inactive (IT) stable. MRS was obtained prior to surgery in patients 1–8 and after treatment in patients 9–24. Data from the AT and IT groups were compared. Knowledge about tumor growth in the AT group was derived from serial MRI demonstrating change in size (surveillance studies in patients with brain tumors) prior to the MRS. Recurrence was validated by histology and/or clinical findings. Of the 16 patients in the AT group, six were treated with radiation, and their clinical picture could be related to this in addition to growth of the tumor. Patients 17–24 were followed for at least 1 year before "no recurrence" was determined. Our pathology assessment at our hospital is largely congruent with the World Health Organization (WHO) [43], and Armed Forces Institute of Pathology (AFIP) [44] systems.

The MR protocol included conventional MRI and proton MRS. The former was performed using spin-echo sagittal T1-weighted images (TR 600 TE 20 ms, two excitations, 24 cm field of view (FOV), 5 mm slice thickness with a 20% interslice gap, and a 128×256 matrix), fast spin-echo (FSE) proton density-weighted images [TR 2000 effective TE 17 ms, 1 excitation, 24 cm FOV, 5 mm slices with a 50% interslice gap, 192×256 matrix, and echo-train length (ETL) four], and FSE T2-weighted images (TR 3200 effective TE 85 ms, one excitation, 24 cm FOV, 5 mm slices with a 50% interslice gap, 192×256 matrix, ETL 8).

Proton MRS was performed using point-resolved spectroscopy (PRESS) [45]. After selecting a 50–100 cc volume, and shimming and water-suppression adjustments, a large data set was obtained using phase-encoding gradients in two directions and the following parameters: TR 1 s TE 65 ms, 16×16 phase encoding matrix, 160 mm FOV, slice thickness 10 mm, 1250 Hz spectral width, two averages and 512 points. Data sets of 1–4.5 cc resolution were acquired.

The data were processed on a workstation using software previously described [46, 47]. The data sets were apodized with a 1.0 Hz Lorentzian filter, Fourier-transformed in the time domain and the two spatial domains and phased. The spectra were first manually phased using spectroscopy analysis software (SAGE) and then the areas of selected metabolite peaks were estimated using PIQABLE. A locally linear baseline estimator was used to subtract the broad components of the baseline prior to peak-area calculations. Metabolite images were generated using SAGE, stored as TIFF files on a workstation, and then transferred to another workstation, to which the conventional images and spectral data were also transferred. The image and spectral data were then processed using software for image analysis from the National Institutes of Health (NIH Image).

The metabolite peaks quantified and analyzed statistically were: choline-containing compounds (Cho), total creatine (tCr), *N*-acetyl-aspartate (NAA), and lipids and/or lactate (L). Means and standard deviations of control metabolite peak values were calculated from all spectra corresponding to control regions in the brain of each patient (contralateral tissues and adjacent tissues uninvolved by tumor). Mean metabolite peak values in tumor tissue were estimated from tumor spectra corresponding to the core of the lesion on T2-weighted images exhibiting the highest Cho peak values (greater than the mean plus two standard deviations of the

Table 1 Clinical data

Case	Age, sex	Site of tumor	Biopsy	Treatment
1	5 years, F	Right parietal	Anaplastic ependymoma	Surgery
2	4 years, M	Posterior cranial fossa	Anaplastic ependymoma	Surgery
3	10 years, M	Brain stem extending to suprasellar region	Fibrillary astrocytoma	Surgery
4	7 years, M	Left thalamic	Pilocytic astrocytoma	Surgery
5	6 years, F	Brain stem	Glioma	Surgery
6	10 months, F	Posterior right temporal	Fibrillary astrocytoma	Surgery
7	9 years, F	Posterior fossa	Pilocytic astrocytoma	Surgery
8	3 years, M	Right optic nerve, optic chiasm, optic radiations to temporal lobes and basal ganglia	Glioma	Surgery
9	15 years, M	Left frontoparietal	Recurrent glioma	Surgery
10	22 years, M	Right thalamic	Recurrent fibrillary astrocytoma	Stereotactic radiotherapy
11	18 years, F	Left temporal	Recurrent anaplastic ependymoma	Radiation seeds; stereotactic radiosurgery
12	24 years, M	Left parieto-occipital	Anaplastic astrocytoma	3 field stereotactic radiosurgery
13	15 years, M	Midline: hypothalamus and chiasmatic cistern	Recurrent medulloblastoma	Craniospinal radiotherapy; chemotherapy
14	8 years, F	Posterior cranial fossa/ supratentorial	Mixed glioma (astrocytic and ependymal)	Conventional
15	17 years, M	Brain stem	Diffusely infiltrating glioma	3 field stereotactic radiosurgery
16	1 year, M	Hypothalamus, optic chiasm	Pilocytic astrocytoma	Chemotherapy
17	7 years, F	Tectum	Not performed	Stereotactic radiotherapy
18	18 years, M	Posterior cranial fossa	Not performed	Stereotactic radiotherapy
19	5 years, F	Left frontal	Ependymoma	Conventional; stereotactic radiosurgery
20	8 years, F	Left frontal	Ependymoma	Radiation
21	17 years, M	Left frontal	Ependymoma	Surgery
22	4 years, F	Right anterior thalamus, optic chiasm	Not performed	Chemotherapy
23	14 years, M	Right temporoparietal	Glioblastoma multiforme	Stereotactic radiosurgery
24	1.5 years, M	Right frontal	Low grade infiltrating glioma	Chemotherapy

control Cho peak values). Whenever only one tumor spectrum was detected, the metabolite values from that spectrum were analyzed statistically. Once the control and tumor spectra to be included in the statistical analysis were identified, all metabolite peak values were standardized to the mean control tCr peak value (as an internal standard) to enable comparison of metabolite levels between patients [41]. Since the area under the tCr peak is relatively constant throughout normal brain tissue [39], its mean value was used as an internal standard or reference peak to estimate relative changes in other metabolites, allowing each patient to serve as his or her own control.

Mean levels of Cho and NAA corresponding to control and tumor regions were compared within the "AT" and the "IT" groups using paired t tests whereas the nonparametric Wilcoxon signed-rank test was used for both tCr and L (Table 2). Mean differences in peak values of any metabolite between AT and IT were evaluated by the unpaired Student's t-test for Cho and NAA and the nonparametric Mann-Whitney U test for tCr and L (Table 2).

Logistic regression was performed to determine the significant predictors of active tumor growth, with the likelihood ratio chi-square test used to assess the significance of each metabolite [48]. Stepwise multiple logistic regression analysis was used to establish the independent multivariate predictors of active tumor growth using stepwise criteria of 0.10 for entry and 0.05 for removal in the final model. Model fit was evaluated by the Hosmer-Lemeshow goodness-of-fit statistic. Data analysis was conducted using the TTEST, NPAR1WAY, and LOGISTIC procedures in SAS version 6.12 (SAS Institute, Cary, N.C.). A two-tailed $P < 0.05$ was considered statistically significant.

Results

The quantitative and statistical analysis of our data is summarized in Table 2. The MRI and MRS findings in

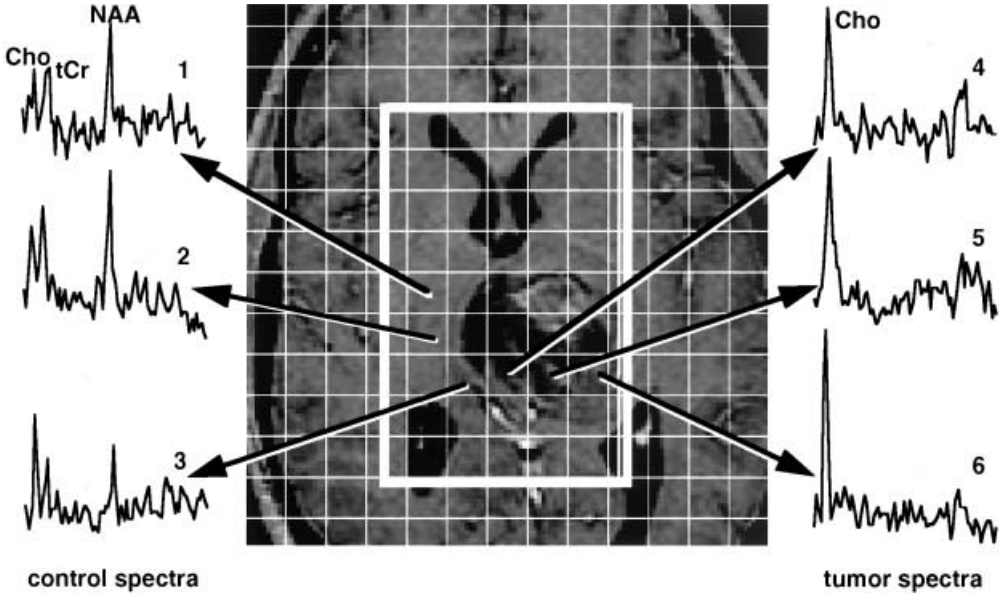

Fig. 1 MRI and proton MRS in a 17-year-old boy with subtotal resection of a midbrain thalamic fibrillary astrocytoma. The contrast-enhanced axial T1-weighted image shows a mass with areas of enhancement. A spectral grid is overlaid on this image. Spectra 4–6, corresponding to the areas of contrast enhancement, show higher choline (Cho) levels than control spectra 1–3 and absence of total creatine (tCr) and *N*-acetyl aspartate (NAA), suggesting tumor recurrence. Biopsy confirmed a diffuse, infiltrating astrocytoma

representative patients are illustrated in Figs. 1 and 2. Fig. 3 shows the inverse relationship between standardized tCr levels and the likelihood of active tumor growth. Three metabolite peaks of biological interest, NAA, Cho and tCr were clearly identifiable in all cases. In some cases, the L peak was also identifiable. Our acquisition protocol yielded spectral data with a high signal-to-noise ratio, as shown in Figs. 1 and 2.

Table 2 presents standardized metabolite peak values of tumor regions as compared to control regions in AT and IT groups. Cho peaks were significantly higher ($P < 0.001$) and tCr and NAA peaks lower ($P < 0.001$) within tumor. The L peak, when identifiable, showed a significant increase in tumor ($P = 0.03$). In the IT group Cho was again significantly increased ($P = 0.02$) and NAA significantly decreased ($P = 0.01$) within tumor. Cho values in the AT group were significantly higher than those in the IT group ($P = 0.05$). The tCr values were significantly different between groups only within tumor regions ($P = 0.02$). The L peak values were signif-

Table 2 Standardized metabolite levels (mean and standard deviation) in active and inactive tumors. *NS* Not significant

Metabolite[a]		Type of tumor		P[e]
		Active[b] (16)	Inactive[c] (8)	
Choline (Cho)	Tumor	2.20 ± 0.81	1.57 ± 0.49	0.05
	Control	0.93 ± 0.21	0.94 ± 0.16	NS
	P[d]	< 0.001	0.02	
Total creatine (tCr)	Tumor	0.23 ± 0.34	0.80 ± 0.61	0.02
	Control	1.00 ± 0.00	1.00 ± 0.00	NS
	P	< 0.001	NS	
N-Acetyl aspartate (NAA)	Tumor	0.73 ± 0.50	0.57 ± 0.47	NS
	Control	1.51 ± 0.55	1.73 ± 0.42	NS
	P	< 0.001	0.01	
Lipid + Lactate (L)	Tumor	1.14 ± 1.86	0.00 ± 0.00	0.04
	Control	0.02 ± 0.07	0. 01 ± 0.02	NS
	P	0.03		NS

[a] All metabolite levels for a patient have been divided by the mean level of total creatine in the control region of that patient
[b] Untreated tumors and nonresponders with recurrent or active tumor ($n = 16$)
[c] Responders with inactive tumor ($n = 8$)
[d] P values comparing active and inactive tumors: unpaired Student's t-test for choline and *N*-acetyl aspartate; Mann-Whitney U-test for creatine and lipid and lactate
[e] P values comparing tumor and control regions: paired t-test for choline and *N*-acetyl aspartate and Wilcoxon signed-rank test for creatine and lipid and lactate

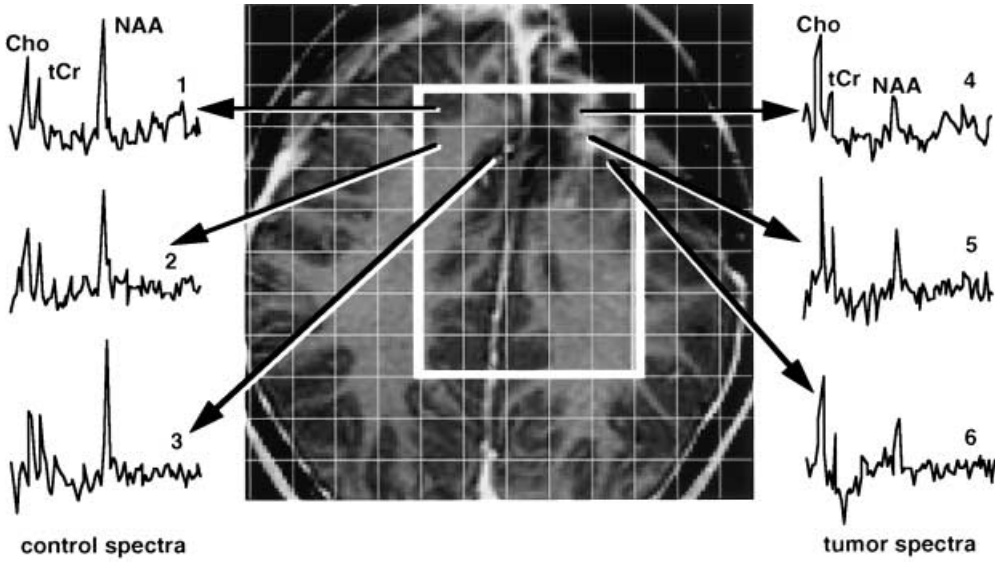

Fig. 2 MRI and MRS of a 5-year-old girl with recurrence of an ependymoma resected 2 years prior to this study. A recurrence was found a year after the initial surgery and the patient underwent a second resection followed by radiation therapy. A contrast-enhanced axial T1-weighted image. Spectra 4–6, from the areas of enhancement show levels of NAA and tCr higher than those typically seen in active tumor, as in Fig. 1. Cho levels are higher than in control spectra 1–3, but not as high as in active tumor, suggesting that the tumor is responsive to the radiation therapy

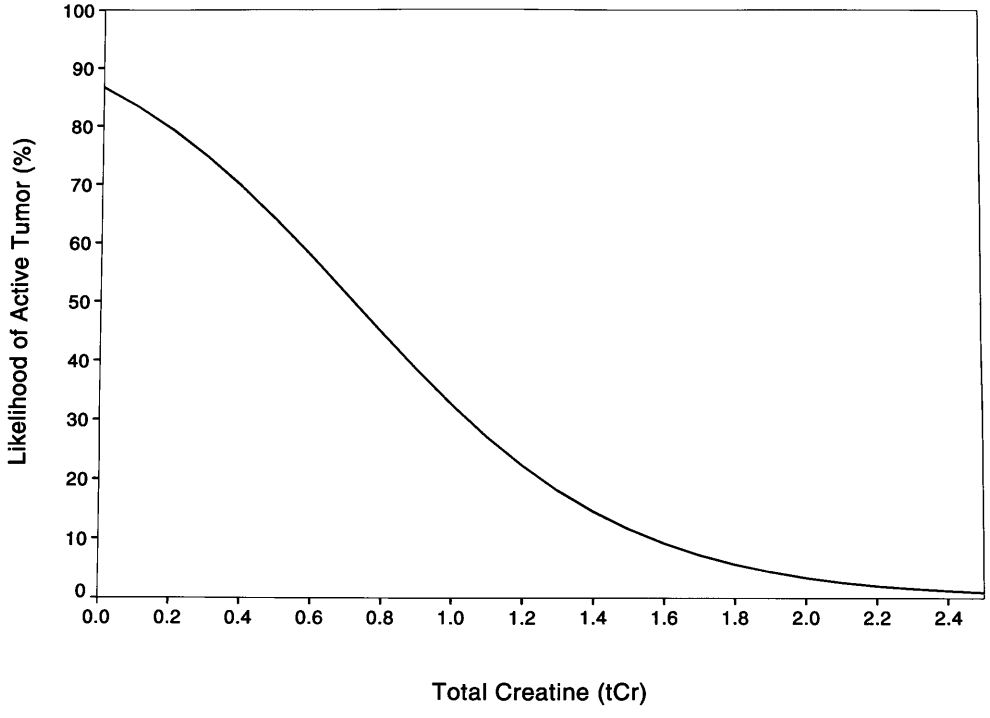

Fig. 3 Estimated probability of active tumor based on standardized levels of tCr. Logistic regression demonstrated a highly significant inverse relationship between standardized tCr and active tumor ($P < 0.01$). The graph shows the likelihood of active tumor based on the total creatine (tCr) level in the tumor region, standardized by dividing it by the mean tCr level in control tissue from the same patient

icantly higher in the AT group ($P = 0.04$); the IT group showed essentially undetectable L peaks.

An inverse relationship between tCr and the estimated likelihood of active tumor is shown in Fig. 3. The stepwise logistic regression analysis established that tCr was the only significant independent multivariate predictor of tumor growth ($P < 0.01$). Cho, NAA, and L did not provide additional predictive information concerning active tumor. The Hosmer-Lemeshow goodness-of-fit test did not reveal departure from model fit ($P = 0.43$).

Discussion

We designed a study to investigate MRS-derived factors that relate to the both active and inactive states of a tumor. We devised what we believe to be appropriate in-

clusion criteria for two groups of patients: those with active (AT) and inactive (IT) tumors. Subsequently, we applied what we take to be an appropriate multivariate statistical analysis to determine which of the MRS-derived, tumor-associated factors were independently predictive of tumor activity. Because we did not analyze tumor progression on MRS, multiple studies were not required. Tumor progression was determined by objective clinical criteria. In addition, we did not investigate tumor response to a specific therapy regime. We therefore included in our analysis patients treated with our currently approved clinical protocols. Our study population was heterogeneous with regard to tumor type and age of the patients. Histologically different neuroepithelial tumors may be expected to differ in their response to treatment. Nevertheless, if they do respond, they become inactive (regardless of how they have been treated) and may be distinguished from active tumors (those newly diagnosed or recurrent). We therefore believe that the study design did not require a specific neuroepithelial tumor type. It was not our intention to make inferences about specific tumor types, such as medulloblastomas, of which there was only one.

Although all the tumors in our study were of neuroepithelial origin, histological subtypes and tumor heterogeneity may influence the distribution of Cho, NAA, tCr and L. We therefore used the Wilk-Shapiro test [49] to evaluate whether any given metabolite showed a significant departure from normality. The Wilk-Shapiro test indicated that the peak values of Cho and NAA were approximately normally distributed, with no serious deviations from homogeneity of variance. However, significant departures from a Gaussian distribution were detected for both tCr and L values. Mean levels of Cho and NAA corresponding to control and tumor regions were therefore compared in the AT and IT groups using paired t tests, whereas the nonparametric Wilcoxon signed-rank test was used for both tCr and L.

Our decision to use TE 65 ms for MRS was made for the following reasons. Most MRS studies of brain tumors have used an echo time of 270 or 272 ms, to detect lactic acid. We were not interested in detecting lactic acid, since it has been shown that it does not necessarily correlate with tumor grade or activity. Nevertheless, lipids might be important as they relate to tumor necrosis (unpublished data), a criterion for grading. It was our pretest hypothesis that an echo time of 65 ms would allow us to null lactic acid, increase sensitivity to lipid and avoid diffusion artifacts and water-suppression failures experienced with PRESS echo times shorter than 65 ms. Lastly, it allowed us to detect the total creatine signal which may not be detected with longer echo times.

Tumor spectra were chosen to have Cho peak values two standard deviations or more above control means. We believe these were the most relevant spectra, since Cho may be low when the volume of interest contains a high degree of necrosis and/or cysts. This has been suggested by studies on solid tumors, which exhibit impressively high Cho [50]. Although we used a discriminative analysis with spectra preselection, the variability of our tumor data is greater than that of our control data (Table 2), reflecting the greater metabolic heterogeneity of the tumors.

Our MRS results using proton two-dimensional CSI support and extend our previous work [5, 7,41]. The present work confirms that spectra acquired within tumors can be differentiated (qualitatively and quantitatively) from those in surrounding non-neoplastic tissue, findings in agreement with those reported elsewhere [9, 19, 20, 38]. Furthermore, this study demonstrates that levels of cell metabolites of biological importance, such as Cho, tCr, NAA, and L, are different in active and inactive tumors. Changes in Cho, tCr and L, could be used to monitor effectiveness of therapy because their values differ significantly according to the response of the tumor. NAA, however, remains unchanged in untreated, active or inactive neoplasms.

The Cho peak

The observed increase in Cho may be attributed to rapid membrane turnover characteristic of neoplasia [51]. This statement, made by other researchers who also need to explain a significant increase in Cho on the basis of a cellular event, deserves further investigation. The peak value is modulated by the responsiveness of tumors to therapy and is in agreement with others [38,52]. Recent evidence supports the notion that Cho increases in regions receiving high doses of radiation and during the acute phase of radiation treatment [53]. An intriguing question is the composition of the Cho peak in vivo and how the constituents relate to neoplastic processes. In vitro work on the canine cerebrum by Barker et al [24] sheds some light on this, suggesting that the Cho peak consists of water-soluble Cho-containing compounds such as phosphocholine and glycerophosphocholine. Others have suggested that the amino acids taurine and hypotaurine, inositol and phosphoethanolamine, may all also be constituents [54].

The NAA peak

NAA, a proposed neuronal marker [55, 56], although shown to be significantly low in tumors, did not qualify as a useful marker for monitoring therapy. This limitation is possibly because many processes other than neoplasia, displace cerebral tissue. Since NAA is found in gray and white matter and in immature neurons [57],

its decrease in tumors may reflect the fact that they replace normal tissue. Where neoplastic tissue invades normal tissue and neoplastic and normal tissue are intermingled, a stronger NAA signal may be detected, probably arising from normal rather than neoplastic tissue. Nevertheless, when the change in Cho is taken together with the change in NAA, demonstration of the extent to which the cerebral tissue is displaced by the tumor may be of clinical value. This can also aid in the identification of sites of radiation necrosis, characteristically low in Cho and NAA [41].

The tCr peak

This work indicates that of the four detectable metabolites, tCr seems to be the strongest predictor of active tumor in the tumor bed (Fig. 3). In most reported studies tCr has not been considered a major peak in tumors because of its low signal. This has been due to the fact that most investigators tailored their MRS protocols to detect lactate by using a long TE (135 or 270 ms). At such long TE, the tCr signal is reduced, due to its T2 decay. We used TE 65 ms, resulting in detection of both lipids and lactate and a strong signal from tCr. We were thus able to observe differences in tCr between active and inactive tumors. It seems that tCr indicates the energy status of the cells in the tissue, apparently low in active tumors. Although speculative, this comment is consistent with the expectation that active tumors should be energy-exhausted due to the fast replication of neoplastic cells. The potential clinical significance of tCr peak as a predictor of tumor growth may lie in screening for energy-exhausted tumors and predicting their response to treatment.

Unlike tCr, Cho was not a significant independent predictor of active tumor. This may not be surprising in view of the phosphorus MRS results suggesting phosphocreatine (PCr) as a strong indicator of tumor metabolic activity [58, 59]. PCr and creatine (Cr) both contribute to tCr. Energy-exhausted tumors also become drained of PCr. Due to energy depletion, Cr, which requires active transport into the cell [60, 61] is prevented from entering the tumor cells, which results in a reduction of the tCr signal. Finally, cell disruption results in a diminution of the tCr signal. This hypothesis needs further exploration and verification, as it introduces a new metabolic index of interest in proton MRS.

The L peaks

L peaks were not detected in all patients. We have considered that the L peaks consist primarily of lipids and secondarily of lactate. Our acquisition protocol, with TE 65 ms, was not optimized to detect lactate. Garwood and colleagues [62, 63] focused attention on lactate and tailored their protocols accordingly, showing in animal studies that lactate is an indicator of tumor metabolic activity, a role that others have disputed [33, 51]. The role of lactate in in vivo MRS of tumors can not to be established until the appropriate pulse sequences and protocols are implemented for detecting lactate in the clinical setting [35, 64, 65]. We set the TE at 65 ms because this was the shortest that could be implemented, to achieve T2 weighting and sensitivity to metabolites with a short TE, such as lipids. Peaks in the 0.8–1.8 ppm range are probably due to aliphatic compounds (lipids) and other macromolecules (proteins). Certain investigators have considered lipids as important indicators of cell activity and indices of tumor grade [19, 66, 67, 68, 69]. Our data are consistent with this: lipids were significantly higher in active tumor than in control regions and in active than in inactive tumors. This change may be of biological significance. A mechanism by which active tumors may release free aliphatic compounds, resulting in an increased in such signals in the proton MR spectrum, needs to be explored. Investigators studying treated tumors implanted in rats, have observed an increase of lipids as a result of tumor and/or treatment-associated necrosis. This opens a new discussion regarding lipid peaks and their value in assessing therapy.

Our data hitherto have suggested the value of MRS in assessing the response of brain tumors to treatment by distinguishing between active and inactive tumors. Others have suggested that in children MRS can provide objective neurochemical information, thereby altering treatment, whenever MRI is indeterminate [70]. Methods other than MRS for assessing brain tumor treatment response may be MR perfusion [71, 72], single-photon emission tomography (SPECT) and positron-emission tomography (PET) [68, 73]. SPECT with thallium-201 chloride (^{201}TlCl) is more sensitive than with PET with F-18 fluorodeoxyglucose to primary or recurrent childhood brain tumors [74], is inexpensive, available in many clinical centers and provides useful information supplementary to CT and MRI, although it may have "false-positive" results in some low-grade gliomas [75]. Technetium-99m-DMSA is superior to 201TlCl in imaging quality, sensitivity to brain tumors and specificity for differentiating benign from malignant tumors [76].

We conclude that: (1) the Cho peak is regulated by responsiveness of brain tumors to treatment; (2) the NAA peak is low regardless of tumor state or response to treatment; (3) the L peaks may help differentiate tumor state; and (4) tCr is the only independent predictor of active tumor growth.

Acknowledgements Research support was provided by American Cancer Society Grant RPG-98–056–01-CCE. We thank S. Vajapeyam PhD for data processing at the initial phase of this work.

References

1. Ries L, Hankey B, Miller B, Hartman A, Edwards B (1991) Cancer statistics review 1973–88. NIH, Bethesda, Md
2. Bleyer W (1993) What can be learned about childhood cancer from "Cancer statistics review 1973–1988"? Cancer 71: 3229–3236
3. Pollack I (1994) Brain tumors in children. N Engl J Med 331: 1500–1507
4. Albright AL (1993) Pediatric brain tumors. CA Cancer J Clin 43: 272–288
5. Tzika AA, Vigneron DB, Ball WS, Dunn RS, Kirks DR (1993) Localized proton MR spectroscopy of the brain in children. JMRI 3: 719–729
6. Tzika A (1995) Localized MR spectroscopy of neurodegenerative disease and tumors. In: E. Faerber (ed) MRI of the central nervous system in infants and children. MacKeith, London, pp 307–328
7. Tzika A, Vigneron D, Dunn R, Nelson S, Ball W (1996) Intracranial tumors in children: small single-voxel proton MR spectroscopy using short and long-echo sequences. Neuroradiology 38: 254–263
8. Wang Z, Sutton L, Canaan A, et al (1995) Proton MR spectroscopy of pediatric cerebellar tumors. AJNR 16: 1821–1833
9. Wang Z, Zimmerman RA, Sauter B (1996) Proton MR spectroscopy of the brain: clinically useful information obtained in assessing CNS diseases in children. Am J Roentgenol 167: 191–199
10. Sutton L, Wehrli S, Gennarelli L, et al (1994) High-resolution ^{1}H-magnetic resonance of pediatric posterior fossa tumors in vitro. J Neurosurg 81: 443–448
11. Sutton L, Wang Z, Gusnard D, et al (1992) Proton magnetic resonance spectroscopy of pediatric brain tumors. Neurosurgery 31: 195–202
12. Segebarth C, Balériaux D, Arnold D, Luyten P, den Hollander J (1987) MR image-guided P-31 MR spectroscopy in the evaluation of brain tumor treatment. Radiology 165: 215–219
13. Byrd SE, Tomita T, Palka PS, Darling CF, Norfray JP, Fan J (1996) Magnetic resonance spectroscopy (MRS) in the evaluation of pediatric brain tumors. Part I: introduction to MRS. J Natl Med Ass 88: 649–654
14. Frahm J, Bruhn H, Gyngell ML, Merboldt KD, Hanicke W, Sauter R (1989) Localized high-resolution proton NMR spectroscopy using stimulated echoes: initial applications to human brain in vivo. Magn Reson Med 9: 79–93
15. Bruhn H, Frahm J, Gungell M, et al (1989) Noninvasive differentiation of tumors with use of localized H-1 MR spectroscopy in vivo: initial experience in patients with cerebral tumors. Radiology 172: 541–548
16. Frahm J, Bruhn H, Hänicke W, Merboldt K, Mursch K, Markakis E (1991) Localized proton NMR spectroscopy of brain tumors using short-echo time STEAM sequences. J Comput Assist Tomogr 15: 915–922
17. van Zijl P, Moonen C, Gillen J, et al (1990) Proton magnetic resonance spectroscopy of small lesions (1 ml) localized inside superficial human tumors. A clinical feasibility study. NMR Biomed 3: 227–232
18. Mader I, Roser W, Hagberg G, et al (1996) Proton chemical shift imaging, metabolic maps, and single voxel spectroscopy of glial brain tumors. Magma 4: 139–150
19. Tien RD, Lai PH, Smith JS, Lazeyras F (1996) Single-voxel proton brain spectroscopy exam (PROVE?SV) in patients with primary brain tumors. Am J Roentgenol 167: 201–209
20. Poptani H, Gupta R, Roy R, Pandey R, Jain V, Chhabra D (1995) Characterization of intracranial mass lesions with in vivo proton MR spectroscopy. AJNR 16: 1593–1603
21. Gill SS, Thomas DGT, van Bruggen N, et al (1990) Proton MR spectroscopy of intracranial tumors: in vivo and in vitro studies. J Comput Assist Tomogr 14: 497–504
22. Kinoshita Y, Kajiwara H, Yokota A, Koga Y (1993) Proton magnetic resonance spectroscopy of brain tumors: an in vitro study. Neurol Med Chir (Tokyo) 33: 350–359
23. Kinoshita Y, Kajiwara H, Yokota A, Roga Y (1994) Proton magnetic resonance spectroscopy of brain tumors: an in vitro study. Neurosurgery 35: 606–613
24. Barker P, Breiter S, Soher B, et al (1994) Quantitative proton spectroscopy of canine brain: in vivo and in vitro correlations. Magn Reson Med 32: 157–163
25. Kinoshita Y, Yokota A (1997) Absolute concentrations of metabolites in human brain tumors using in vitro proton magnetic resonance spectroscopy. NMR Biomed 10: 2–12
26. Florian C, Preece N, Bhakoo K, Williams S (1996) Characteristic metabolic profiles revealed by 1H NMR spectroscopy for three types of human brain and nervous system tumours. NMR Biomed 8: 253–264
27. Luyten P, Marien A, Heidel W, et al (1990) Metabolic imaging of patients with intracranial tumors: H-1 MR spectroscopic imaging and PET. Radiology 176: 791–799
28. Alger J, Frank J, Bizzi A, et al (1990) Metabolism of human gliomas: assessment with H-1 MR spectroscopy and F-18 fluorodeoxyglucose PET. Radiology 177: 633–641
29. Arnold D, Shoubridge E, Emrich J, Feindel W, Villemure J (1989) Early metabolic changes following chemotherapy of human gliomas: in vivo demonstrated by phosphorus magnetic resonance spectroscopy. Invest Radiol 24: 958–961
30. Segebarth C, Balériaux D, Luyten P, den Hollander J (1990) Detection of metabolic heterogeneity of human intracranial tumors in vivo by H-1 NMR spectroscopic imaging. Magn Reson Med 13: 62–76
31. Fulham MJ, Bizzi A, Dietz MJ, Shih HH, Raman R (1992) Mapping of brain tumor metabolites with proton MR spectroscopic imaging: clinical relevance. Radiology 185: 675–686
32. Negandank WG, Sauter R, Brown TR, et al (1996) Proton magnetic resonance spectroscopy in patients with glial tumors: a multicenter study. J Neurosurg 84: 449–458
33. Barker P, Glickson J, Bryan R (1993) In vivo magnetic resonance spectroscopy of brain tumors. Topics Magn Reson Imaging 5: 32–45
34. Manton DJ, Lowry M, Blackband SJ, Horsman A (1995) Determination of proton metabolite concentrations and relaxation parameters in normal human brain and intracranial tumours. NMR Biomed 8: 104–112
35. Henriksen O (1995) In vivo quantitation of metabolite concentrations in the brain by means of proton MRS. NMR Biomed 8: 139–148
36. Castillo M, Kwock L, Mukherji SK (1996) Clinical applications of proton MR spectroscopy. AJNR 17: 1–15
37. Poptani H, Gupta RK, Jain VR, Roy R, Pandey R (1995) Cystic intracranial mass lesions: possible role of in vivo MR spectroscopy in differential diagnosis. Magn Reson Imaging 13: 1019–1029
38. Byrd SE, Tomita T, Palka PS, Darling CF, Norfray JP, Fan J (1996) Magnetic resonance spectroscopy (MRS) in the evaluation of pediatric brain tumors. Part II: clinical analysis. J Natl Med Ass 88: 717–723

39. Preul MC, Caramanos Z, Collins DL, et al (1996) Accurate, noninvasive diagnosis of human brain tumors by using proton magnetic resonance spectroscopy. Nat Med 2: 323–325
40. Brown T, Kincaid B, Ugurbil K (1982) NMR chemical shift imaging in three dimensions. Proc Natl Acad Sci USA 79: 3523–3526
41. Tzika AA, Vajapeyam S, Barnes PD (1997) Multivoxel proton MR spectroscopy and hemodynamic MRI of childhood brain tumors: preliminary observations. AJNR 18: 203–218
42. Wald LL, Nelson SJ (1997) Serial proton magnetic resonance spectroscopy imaging of glioblastoma multiforme after brachytherapy. J Neurosurg 87: 525–34
43. Kleihues P, Burger PC, Scheithauer BW (1993) Histological typing of tumours of the central nervous system, 2nd edn. Springer, Berlin Heidelberg New York, p. 112
44. Burger P, Scheithauser B (1994) Atlas of tumor pathology: tumors of the central nervous system. Armed Forces Institute of Pathology, Washington
45. Bottomley PA (1987) Spatial localization in NMR spectroscopy in vivo. Ann N Y Acad Sci 508: 333–348
46. Nelson S, Brown T (1987) A new method for automatic quantification of 1-D spectra with low signal to noise ratio. J Magn Reson 75: 229–243
47. Nelson S, Brown T (1989) A study of the accuracy of quantification which can be obtained from 1-D NMR spectra using the PIQABLE algorithm. J Magn Reson 84: 95–109
48. Hosmer DW, Lemeshow S (1989) Applied logistic regression. Wiley, New York, pp 38–57
49. Shapiro SS, Wilk MB (1965) An analysis of variance test for normality (complete samples). Biometrika 52: 591–611
50. Sijens PE, van Dijk P, Oudkerk M (1994) Correlation between choline level and Gd-DTPA enhancement in patients with brain metastases of mammary carcinoma. Magn Reson Med 32: 549–555
51. Kugel H, Heindel W, Ernestus RI, Bunke J, du Mesnil R, Friedman G (1992) Human brain tumors: spectral patterns detected with localized H-1 MR spectroscopy. Radiology 183: 701–709
52. Sijens PE, Vecht CJ, Levendag PC, van Dijk P, Oudkerk M (1995) Hydrogen magnetic resonance spectroscopy follow-up after radiation therapy of human brain cancer. Unexpected inverse correlation between the changes in tumor choline level and post-gadolinium magnetic resonance imaging contrast Invest Radiol 30: 738–744
53. Szigety S, Allen P, Huyser-Wierenga D, Urtasun R (1993) The effect of radiation on normal human CNS as detected by NMR spectroscopy. Int J Radiat Oncol Biol Phys 25: 695–701
54. Remy C, Arus C, Ziegler A, et al (1994) In vivo, ex vivo, and in vivo one-and two-dimensional nuclear magnetic resonance spectroscopy of an intracerebral glioma in rat brain: assignment of resonance. J Neurochem 62: 166–179
55. Tallan HH (1957) Studies on the distribution of N-acetyl-L-aspartic acid in brain. J Biol Chem 224: 41–45
56. Birken DL, Oldendorf WH (1989) N-Acetyl-L-aspartic acid: a literature review of a compound prominent in ^{1}H-NMR spectroscopic studies of brain. Neurosci Biobehav Rev 13: 23–31
57. Urenjak J, Williams SR, Gadian DG, Noble M (1992) Specific expression of N-acetylaspartate in neurons, oligodendrocyte-type-2 astrocyte progenitors, and immature oligodendrocytes in vitro. J Neurochem 59: 55–61
58. Ross B, Higgins R, Boggan J, Knittel B, Garwood M (1988) 31P NMR spectroscopy of the in vivo metabolism of an intracerebral glioma in the rat. Magn Reson Med 6: 403–417
59. Heindel W, Bunke J, Glathe S, Steinbrich W, Mollevanger L (1988) Combined 1H-MR imaging and localized 31P-spectroscopy of intracranial tumors in 43 patients. J Comput Assist Tomogr 12: 907–916
60. Bennett SE Bevington A Walls J (1994) Regulation of intracellular creatine in erythrocytes and myoblasts: influence of uraemia and inhibition of Na, K-ATPase. Cell Biochem Funct 12: 99–106
61. Guimbal C Kilimann MW (1993) A Na(+)-dependent creatine transporter in rabbit brain, muscle, heart, and kidney. cDNA cloning and functional expression. J Biol Chem 268: 8418–21
62. Ross BD, Merkle H, Hendrich K, Staewen RS, Garwood M (1992) Spatially localized in vivo 1H magnetic resonance spectroscopy of an intracerebral rat glioma. Magn Reson Med 23: 96–108
63. Terpstra M, High WB, Luo Y, de Graaf RA, Merkle H, Garwood M (1996) Relationships among lactate concentration, blood flow and histopathologic profiles in rat C6 glioma. NMR Biomed 9: 185–194
64. Duyn JH, Frank JA, Moonen CT (1995) Incorporation of lactate measurement in multi-spin-echo proton spectroscopic imaging. Magn Reson Med 33: 101–107
65. Thomas MA, Ryner LN, Mehta MP, Turski PA, Sorenson JA (1996) Localized 2D J-resolved 1H MR spectroscopy of human brain tumors in vivo. J Magn Reson Imaging 6: 453–459
66. Yoshino E, Ohmori Y, Imahori Y, et al (1996) Irradiation effects on the metabolism of metastatic brain tumors: analysis by positron emission tomography and 1H-magnetic resonance spectroscopy. Stereotact Funct Neurosurg 66: 240–259
67. Sijens P, Levendag P, Vecht C, van Dijk P, Oudkerk M (1996) 1H MR spectroscopy detection of lipids and lactate in metastatic brain tumors. NMR Biomed 9: 65–71
68. Slosman DO, Lazeyras F (1996) Metabolic imaging in the diagnosis of brain tumors. Curr Opin Neurol 9: 429–435
69. Furuya S, Naruse S, Ide M, et al (1997) Evaluation of metabolic heterogeneity in brain tumors using 1H-chemical shift imaging method. NMR Biomed 10: 25–30
70. Norfray JF, Tomita T, Byrd SE, Ross BD, Berger PA, Miller RS (1999) Clinical impact of MR spectroscopy when MR imaging is indeterminate for pediatric brain tumors. Am J Roentgenol 173: 119–125
71. Gaa J, Warach S, Wen P, Thangaraj V, Wielopolski P, Edelman RR (1996) Noninvasive perfusion imaging of human brain tumors with EPISTAR. Eur Radiol 6: 518–522
72. Knopp EA, Cha S, Johnson G, Mazumdar A, Golfinos JG, Zagzag D, Miller DC, Kelly PJ, Kricheff II (1999) Glial neoplasms: dynamic contrast-enhanced T2*-weighted MR imaging. Radiology 211: 791–798
73. Derlon JM (1998) The in vivo metabolic investigation of brain gliomas with positron emission tomography. Adv Techn Standards Neurosurg 24: 41–76
74. Maria BL, Drane WE, Mastin ST, Jimenez LA (1998) Comparative value of thallium and glucose SPECT imaging in childhood brain tumors. Pediatr Neurol 19: 351–357
75. Tamura M, Shibasaki T, Zama A, Kurihara H, Horikoshi S, Ono N, Oriuchi N, Hirano T (1998) Assessment of malignancy of glioma by positron emission tomography with 18F-fluorodeoxyglucose and single photon emission computed tomography with thallium-201 chloride. Neuroradiology 40: 210–215
76. Hirano T, Otake H, Kazama K, Wakabayashi K, Zama A, Shibasaki T, Tamura M, Endo K (1997) Technetium-99 m(V)-DMSA and thallium-201 in brain tumor imaging: correlation with histology and malignant grade. J Nucl Med 38: 1741–1749